

ORNL  
MASTER COPY

820513

OCT 14 1982

ORNL-5885

**oml**

OAK  
RIDGE  
NATIONAL  
LABORATORY



## Design Study of a Flexible Diaphragm

M. E. Whalley<sup>1</sup>  
J. G. Morgan *ilr*



OPERATED BY  
UNION CARBIDE CORPORATION  
FOR THE UNITED STATES  
DEPARTMENT OF ENERGY



**ORNL-5885**  
**Dist. Category UC-86**  
**(Applied)**

Contract No. W-7405-eng-26

**Consolidated Fuel Reprocessing Program**

**DESIGN STUDY OF A FLEXIBLE DIAPHRAGM**

M. E. Whatley

and

J. G. Morgan

Fuel Recycle Division

Oak Ridge National Laboratory

Oak Ridge, Tennessee 37830

Date Published - October 1982

**OAK RIDGE NATIONAL LABORATORY**  
Oak Ridge, Tennessee 37830  
operated by  
**UNION CARBIDE CORPORATION**  
for the  
**DEPARTMENT OF ENERGY**



## CONTENTS

ABSTRACT .....	1
1. INTRODUCTION.....	1
2. CALCULATIONS.....	1
2.1 Problem Definition .....	1
2.2 Computer Codes .....	5
3. THE DIAPHRAGM STUDY .....	6
3.1 Existing Diaphragm.....	7
3.2 Six Extrema Cases, Small Outside Radius .....	7
3.3 Larger Radius Diaphragms.....	12
3.4 Alternate Design .....	15
3.5 Scaled Design .....	16
3.6 Reverse Displacement .....	16
3.7 Measured Stresses .....	19
4. CONCLUSIONS .....	20
5. ACKNOWLEDGMENTS.....	21
REFERENCES .....	21
APPENDIX A – PROGRAM FOR MATRIX GENERATION.....	A-1
APPENDIX B – MATRIX PROGRAM OUTPUT .....	B-1



# DESIGN STUDY OF A FLEXIBLE DIAPHRAGM

M. E. Whatley

and

J. G. Morgan

## ABSTRACT

A design study was made to meet the requirements for a diaphragm for a rotary seal at the discharge end of the Consolidated Fuel Reprocessing Program's prototypic voloxidizer. Using a computer program called NEPSAP, the study examined thickness, outer radius, corrugation wavelength and corrugation amplitude as variables, and established the general effect of each on stiffness and stresses. The result comprises a basis for the selection of diaphragms for similar applications. Limited experimental measurements of stress validate the stress values calculated by NEPSAP.

## 1. INTRODUCTION

A proposed step in a fuel reprocessing plant is voloxidation, which converts  $\text{UO}_2$  to  $\text{U}_3\text{O}_8$  and releases tritium for isolation from the rest of the process. The rotary calciner voloxidizer design features a mechanical rotating seal on each end of the calciner to isolate the contents from the cell atmosphere. This seal consists of a monolithic graphite ring bearing against the rotating calciner flange and is supported by a thin metal corrugated diaphragm. The outer diameter of the diaphragm is fixed to the stationary breeching housing. There must be no horizontal surfaces to collect fuel inventory, and the assembly must accommodate misalignment and horizontal thermal expansion of the drum. The diaphragm can be so positioned that its inner diameter will be required to move a maximum distance of 1.5 in. during heat up. This report describes a detailed design study undertaken to determine the optimum configuration for such a diaphragm. Although this work was directed primarily toward meeting the need for a voloxidizer seal, the concept could be applied to the general design problem of a gas seal for large rotating equipment.

## 2. CALCULATIONS

### 2.1 Problem Definition

Analysis was undertaken after a diaphragm designed from intuitive principles failed. From the initial effort, we established a general form for the design of acceptable diaphragms which limited the range of designs considered. We had also seen a failure, which told us in measure, what to look for in analysis. The diaphragm would be made from a single sheet of fairly ductile metal as thin as consistent with welding, handling, and fabrication considerations. It would conform to axial symmetry with circumferential corrugations or waves such that the circle at the inner radius fell in the same plane as the circle at the outer radius. A section at any radius would show the same sinusoid type pattern that might or

might not have flat regions at the inner and/or outer radius, with all waves of the same amplitude above and below the reference plane, and with the same nominal wavelength. Variations from these simple specifications were actually considered at different times in the study, but since no significant advantage was established they were abandoned and will not be further discussed.

The material used for the fabrication of all experimental diaphragms was 304L stainless steel. This material met all requirements reasonably well, and a cursory search revealed no potentially superior material. The physical properties of 304L stainless steel were used in all analyses.

Early studies (examining diaphragms of 10, 18, and 30 mils) considered thickness as a parameter. It was found that the stiffness of the diaphragm (the force per unit displacement) increased almost as the square of the thickness but that the stress in the diaphragm changed less drastically. The circumferential stresses were somewhat less for thinner diaphragms but the radial stresses were somewhat greater. Since practical considerations precluded diaphragms thinner than  $\sim 18$  mils, this thickness was used as a standard for all subsequent calculations.

It was then necessary to describe mathematically the corrugation pattern of the diaphragms. The original drawings from which the first diaphragms were fabricated showed the curves as arcs of circles. It was clear, however, from examining the diaphragms that the waveform only approximately followed the drawings. The springiness of the material while it is being worked into a form does not allow these waves of relatively low amplitude to be made with precision sufficient to distinguish between circles, parabolas, or a sinewave. An early analysis was done using circular arcs to describe the corrugations, but when it became desirable to make parametric studies it was found that the amplitude could not be varied conveniently.

Since the selection of the mathematical form to describe the diaphragm in analysis was considered of sufficient importance to consume considerable programmatic effort and was changed once between the early work and the later nonlinear analysis, a more quantitative comparison of the alternatives may be of interest to the reader. It was required that a transverse section along a radius would show the corrugations as a wave with equal amplitude above and below a reference plane. The wave would fall in the reference plane at the inner and outer bounds where the slope would be zero. Hence, at the approach to the bounds the pattern must be broken, but it was required that a curve of the form used in the pattern be used to fold the curve into the reference plane and that the curve be continuous and have continuous first derivatives at the juncture. This manipulation of the curve is shown in Fig. 1 for the parabolic representation.

The equations used to form the patterns are:

for a parabola,

$$\frac{y}{a} = 1 - \left( \frac{2X}{\lambda} \right)^2 ,$$

for a trigonometric wave,

$$\frac{y}{a} = \cos \left( \frac{\pi X}{\lambda} \right) ,$$

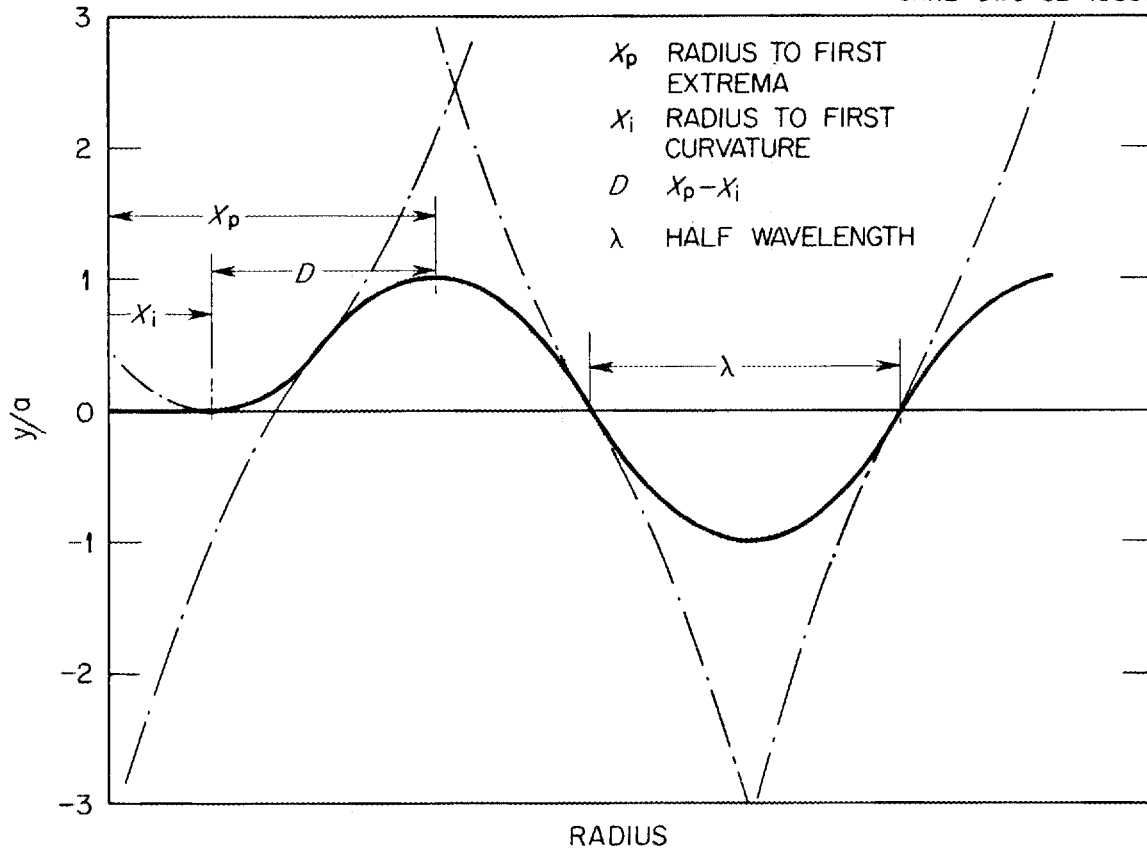


Fig. 1. Parabolic representation of a diaphragm.

and for a circle,

$$\frac{y}{a} = \frac{-1 + \left(\frac{2a}{\lambda}\right)^2 + \sqrt{\left[1 - \left(\frac{2a}{\lambda}\right)^2\right]^2 + 4\left(\frac{2a}{\lambda}\right)^2 \left[1 - \left(\frac{2X}{\lambda}\right)^2\right]}}{2\left(\frac{2a}{\lambda}\right)^2},$$

where

$y$  = distance above the reference plane,

$a$  = the maximum  $y$  (the amplitude),

$X$  = distance from an extrema,

$\lambda$  = half wavelength, or distance between nodes.

These equations are actually correct only for the positive extrema. The negative extrema, in the case of a parabola or a circle, must be generated by the appropriate changes in signs.

Note that the normalized quantity  $y/a$  is independent of  $a$  for the parabola and the trigonometric wave, but when the wave is formed from circular segments, the group  $2a/\lambda$  is prominent. Table 1 shows the values of  $y/a$  vs  $2X/\lambda$  for the parabola, the trigonometric form, and the

**Table 1. Comparison of corrugation geometry**

$\frac{2X}{\lambda}$	$\lambda/a$				
	Circle ( $2a/\lambda$ )			Parabola	Trigonometric
	0.5	0.1	0.02		
0.1	0.235	0.192	0.190	0.190	0.156
0.2	0.421	0.362	0.360	0.360	0.309
0.3	0.571	0.531	0.510	0.510	0.454
0.4	0.693	0.642	0.640	0.640	0.588
0.5	0.791	0.752	0.750	0.750	0.707
0.6	0.869	0.841	0.840	0.840	0.809
0.7	0.927	0.911	0.910	0.910	0.891
0.8	0.968	0.960	0.960	0.960	0.951
0.9	0.992	0.990	0.990	0.990	0.988
1.0	1.000	1.000	1.000	1.000	1.000

circle for three values of  $2a/\lambda$ . For the larger values of  $2a/\lambda$  the circle is seen to deviate from the other two, but as  $2a/\lambda$  gets small (for interesting diaphragms it is  $<0.2$ ) the circle approaches the parabola. Further note that in a typical case with a 0.2-in. amplitude, the thickness of the diaphragms (0.018 in.) gives a  $\Delta y/a$  of 0.09, which is generally greater than the difference between models.

A difference between models is also seen in the radial distance before the first extrema where curvature of the diaphragm must start (Fig. 1). For the parabola, the starting point is  $0.707\lambda$  and for the trigonometric form it is  $0.666\lambda$ , but for the circular wave it is a function of  $2a/\lambda$ . For a circular wave, the distance before first extrema is:

$$0.5 \sqrt{2.0 + (2a/\lambda)^2}$$

At  $2a/\lambda = 0.5$  the distance is  $0.75\lambda$ , and as  $2a/\lambda$  decreases, the distance approaches that for a parabola.

Comparable cases were run in the linear mode using a parabolic and a circular representation of the diaphragm and no significant difference was noted. All work reported here used the parabolic form. Analysis of the corrugation waveform as a trigonometric function resulted in a diaphragm that was 80% as stiff as a parabolic function. Examination of the stress patterns showed subtle changes between the two functions but there were no major differences, which indicates that small manufacturing variations will somewhat influence diaphragm characteristics. It also indicates that analysis based on a parabolic waveform has not confined itself to a uniquely preferable form but is, in a sense, conservative.

## 2.2 Computer Codes

For the calculation of stresses in candidate diaphragms, we solicited the assistance of personnel in the Computer Sciences Division and the UCC-ND Engineering Division who pursue stress analysis as their major occupation. We discovered quickly that ours was not a trivial problem for which solutions existed and that to deploy existing computer programs to obtain solutions would require some development. The initial work was done by S. K. Iskander using the ADINA<sup>1</sup> program in a linear mode. When it became clear that our problem was highly nonlinear,<sup>2</sup> this program was abandoned in favor of the NEPSAP program, introduced to us by John Mayhall who developed the form for the computer input and setup and executed several of the early cases. NEPSAP is a three-dimensional finite element program for the nonlinear thermo-elastic-plastic and creep analysis of arbitrary structures undergoing large deformations.<sup>3</sup> Our diaphragm problem was axisymmetric, and hence, only two dimensional, was isothermal, and (except for one special case) was run in the elastic range of the material. Because NEPSAP is a very general program, the input is rather involved, but since our problem used only a fraction of the program's capability, it was possible to establish a standard input in which particular numbers were changed to define the different cases.

The most difficult part of preparing the input to NEPSAP was the generation of the  $x,y$  coordinates for each of about a thousand nodes necessary to define the diaphragm surfaces and the elements required for the calculation. The nodes were numbered from the inner radius to the outer, alternating from the bottom surface to the top such that all odd numbered nodes were on the bottom. To do this expeditiously, a short computer program was written to be executed on the PDP-10. This program (listed in Appendix A) accepts as input the number of extrema, the inner radius, the radius to the first extrema, the outer radius, the half wavelength, the amplitude of the waves, the diaphragm thickness, the ratio of element length to diaphragm thickness, and a case number. It generates the form of the diaphragm and lays out nodes and elements such that the elements are all the same length along the curve. Its output is stored in a retrievable file in a format compatible with NEPSAP input. The first part of a typical output is shown in Appendix B. This particular diaphragm required 1168 nodes. For each radius location on the surface there is a corresponding point on the vertical axis. These values are positive as the corrugation bends upward above the original inside radius (IR) position. An increment size of twice the thickness was used throughout the study. We tried a coarser matrix in one case (12) with a length of four times the thickness. There was no detectable loss of accuracy.

NEPSAP input also allows specifications of each incremental load. It was necessary in some calculations to experiment with nonuniform application of the load to accommodate acutely sensitive regions of stiffness.

The output from NEPSAP is voluminous. For each load increment (typically 20), the output listed for each nodal point: its displaced coordinates, strain in three directions, normal stress and shear stresses in three directions, Hencky Von Mises stresses, and other information relating to the progress of the calculation. This output was stored on microfiche. NEPSAP also presented all of this information in an unformatted mode to an output which could be recorded on magnetic tape. Techniques to use this output were developed about halfway through our effort and about half of our calculations were (and are) available for postprocessing.

In order to compare diaphragms in our study, the load curve of force vs displacement and the surface stresses at 1.5-in. displacement were considered. A computer program was developed to extract information from the NEPSAP output tape, printing top and bottom radial and circumferential stresses at the first load increment (essentially the linear case) and interpolating between load increments to give a displacement of 1.5 in. The program also generated a plot of these stresses vs diaphragm radius and Lissajous plots of stress vs corrugation wave.

### 3. THE DIAPHRAGM STUDY

The inner radii of all diaphragms studied were fixed (dictated by the voloxidizer drum diameter) at 14.5 in. As discussed in Sect. 2.1, the 18-mil thickness was chosen in all cases except the 3/4 (0.75)-scale model, case 14. The four different diaphragm configurations used in the study are shown schematically in Fig. 2. Figure 2(a) is an existing diaphragm, case 13, with four extrema having flats at the inside radius (IR) and outside radius (OR). All

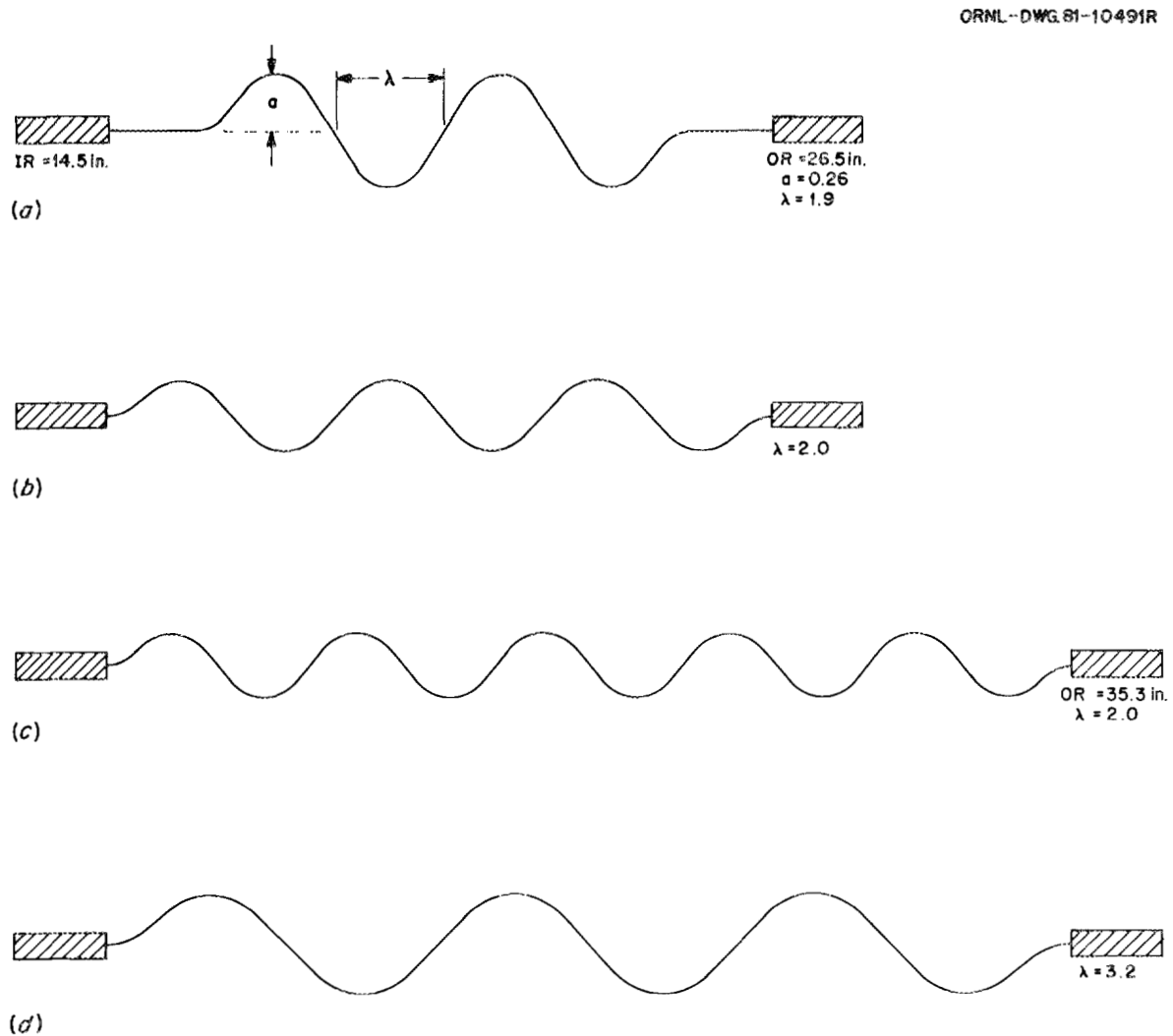


Fig. 2. Diaphragm models.

other cases considered continuous corrugations across the diaphragm; therefore, the distance to the first extrema was fixed by the geometry. Figure 2(b) is a series of cases (1, 2, 4, 5, 6, and 11) with a half wavelength of 2 in. and six extrema resulting in an OR approximately the same as the OR for case 13; the amplitude was varied from 0.05 in. to 0.75 in. A larger OR with ten extrema is shown in Fig. 2(c). Results were obtained for three different amplitudes, cases 12, 16, and 17. Figure 2(d) is similar to Fig. 2(c) except six extrema were considered and the amplitude varied from 0 (flat plate) to 0.35 in., cases 50 through 56. The effect of half wavelength can then be determined by comparing cases in Figs. 2(c) and (d) having the same amplitude (i.e., cases 17 and 51). The effect of scaling using case 14, which is a 0.75-scale of case 12, and the effect of reversing the direction of displacement in cases 12 and 13 were also considered. All case dimensions are given in Table 2.

### 3.1 Existing Diaphragm

A diaphragm, already on hand, was used in the proof testing of the seal concept. The diaphragm (Fig. 3) operated satisfactorily under conditions of tilt and eccentricity,<sup>4</sup> but under repeated flexure it developed indentations and eventually failed; therefore, it became a reference unacceptable case. Figure 3 is a photograph of this diaphragm. Note the inner and outer metal weld rings. The graphite ring, at the inner diameter, acts as a gas seal against a rotating flange on the voloxidizer drum. An analysis was made to determine the stresses and the force required to displace the diaphragm longitudinally. Design limitations on the thrust bearings that align the inlet drive mechanism limit this force to 400 lb.

A profile of the diaphragm, shown in Fig. 2(a), shows four extrema and a flat region at the inner and outer radii. The force required to displace the inner diameter of the diaphragm 1.5 in. was calculated to be 375 lb. Figure 4 (case 13, existing diaphragm) is a composite plot of the surface stresses at 1.5 in. in displacement, which are plotted as a function of radius with the profile of the diaphragm shown at the bottom of the plot. The direction of deflection is upward at the IR. Near the first extrema the calculated radial stress is close to 60 000 psi. There is also a high stress at the inner and outer radii where the diaphragm is clamped to the sharp edged weld rings. The plots of the radial stresses at the top and bottom surfaces are essentially mirror images, one in compression while the other is in tension at a given radius. Circumferential stresses were lower than radial but still probably unacceptably high.

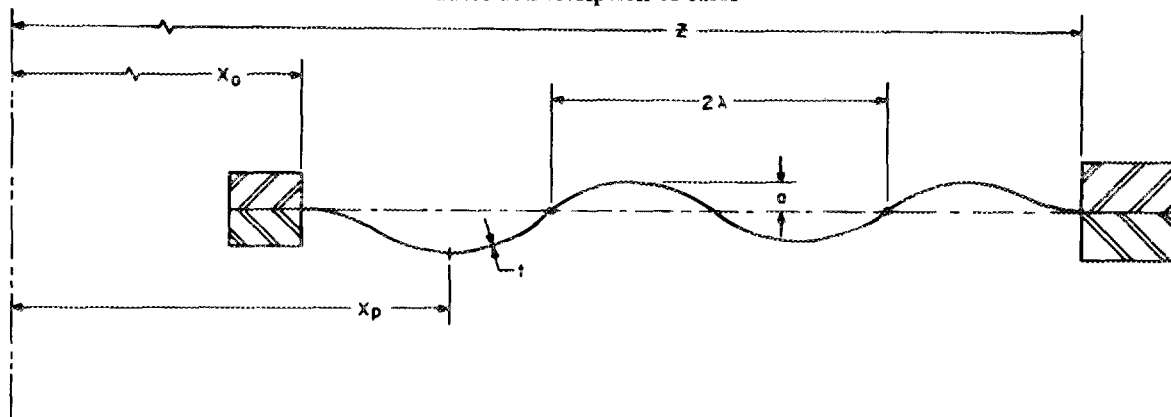
The criteria for acceptable stress is still rather nebulous, but data<sup>5</sup> on fatigue of 304L stainless steel show that cyclic stresses over ~35 000 psi eventually lead to failure and that a cyclic stress of 55 000 will cause failure in 10 000 cycles. Although our application requires survival over only a few hundred cycles, justifying high design stresses, there are uncertainties, such as how well the manufactured diaphragm will conform to the geometry of the model. Our arbitrary target was a maximum stress of <30 000 psi.

### 3.2 Six Extrema Cases, Small Outside Radius

We next considered cases of a diaphragm with corrugations extending over all of the available radial distance, Fig. 2(b). A half wavelength of 2.0 in. and six extrema resulted in an OR of 27.3 in., which is close to that of the existing diaphragm (26.5 in.). Calculations were made on six cases in which the amplitude was varied from 0.05 in. to 0.75 in., and the

Table 2. Description of cases

ORNL DWG. 81-1423



Case	Variable description (in.)						
	Inner radius ( $X_0$ )	Half wavelength ( $\lambda$ )	Amplitude ( $a$ )	First extrema ( $X_p$ )	Number of extrema ( $N$ )	Outer radius ( $Z$ )	Thickness ( $t$ )
1	14.5	2	0.303	15.91	6	27.338	0.018
2	14.5	2	0.75	15.91	6	27.338	0.018
3	14.5	1	0.151	15.21	12	27.338	0.018
4 <sup>a</sup>	14.5	2	0.20	15.915	6	27.338	0.018
5 <sup>a</sup>	14.5	2	0.1	15.915	6	27.338	0.018
6 <sup>a</sup>	14.5	2	0.05	15.915	6	27.338	0.018
7	14.5	1	0.1	15.21	12	27.338	0.018
9	14.5	3.75	0.375	17.170	3	27.338	0.018
11 <sup>a</sup>	14.5	2	0.15	15.91	6	27.338	0.018
12	14.5	2	0.2	15.91	10	35.338	0.018
13 <sup>b</sup>	14.5	1.874	0.262	17.886	4	26.499	0.018
14 <sup>c</sup>	10.88	1.5	0.15	11.936	10	26.50	0.014
16 <sup>d</sup>	14.5	2	0.15	15.915	10	35.338	0.018
17 <sup>d</sup>	14.5	2	0.25	15.915	10	35.338	0.018
50 <sup>e</sup>	14.5	—	—	—	—	35.338	0.018
51 <sup>f</sup>	14.5	3.248	0.25	16.800	6	35.338	0.018
52 <sup>f</sup>	14.5	3.248	0.35	16.800	6	35.338	0.018
54 <sup>f</sup>	14.5	3.248	0.18	16.800	6	35.338	0.018
55 <sup>f</sup>	14.5	3.248	0.15	16.800	6	35.338	0.018
56 <sup>f</sup>	14.5	3.248	0.13	16.800	6	35.338	0.018

<sup>a</sup>Varying amplitude from case 2.<sup>b</sup>First diaphragm.<sup>c</sup>Three-fourths (0.75)-scale version of case 12.<sup>d</sup>Varying amplitude from case 12.<sup>e</sup>Flat plate.<sup>f</sup>Varying amplitude from case 51.



Fig. 3. Existing diaphragm.

results are shown in Fig. 5. The largest amplitude case (0.75 in.) was prohibitively stiff (required a large force for a given displacement). In contrast, the smallest amplitude case (0.05 in.) gave a very low force requirement for the first 0.7-in. extension but then curved sharply upward exceeding 400 lb at the 1-in. displacement. The best amplitude appears to be 0.15 in. (case 11). The stresses for this case were calculated at 1.5-in. extension, and the results are shown in Fig. 6. The radial stress remained high at the IR but improved (50 000 vs

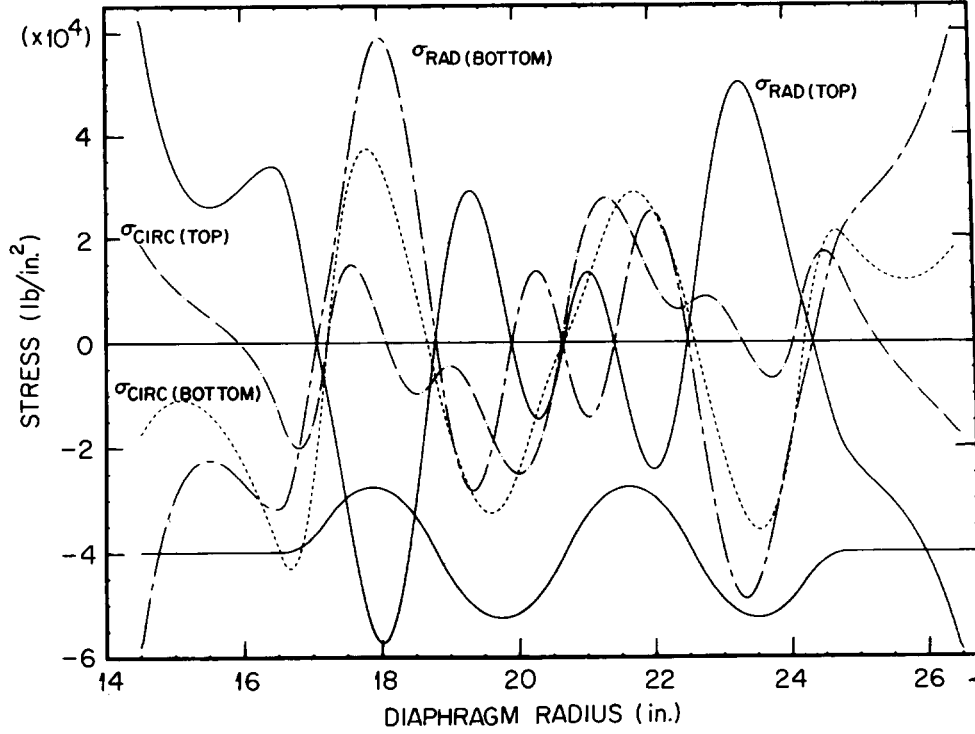


Fig. 4. Case 13, existing diaphragm.

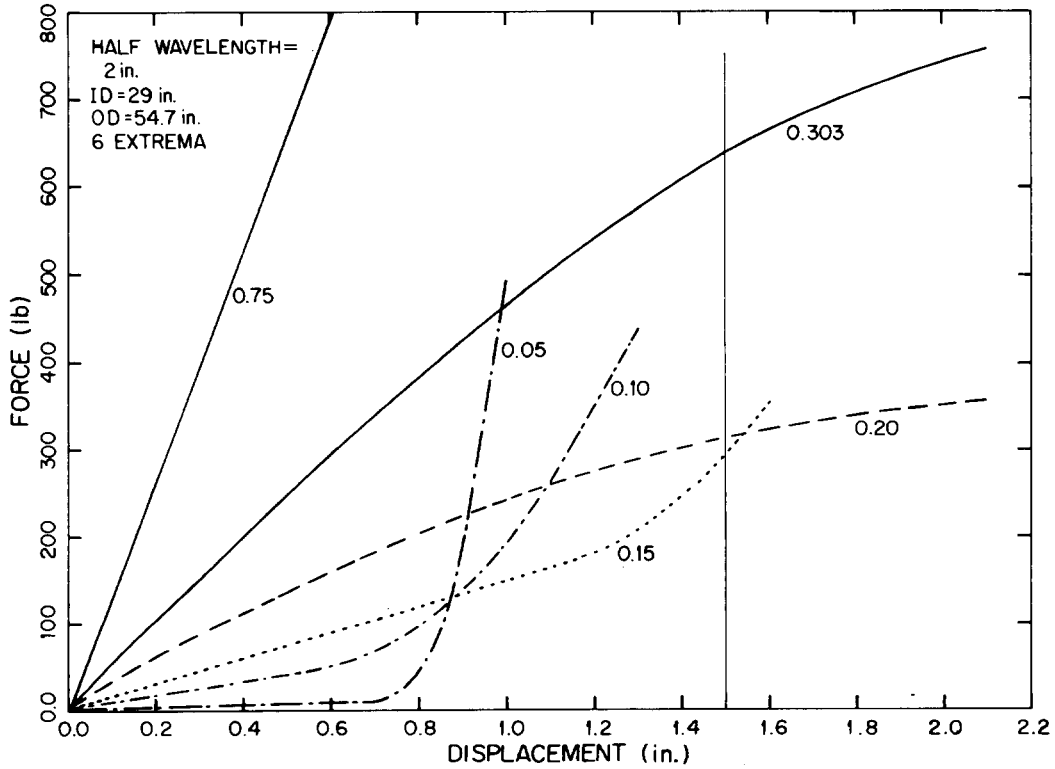


Fig. 5. Force requirement.

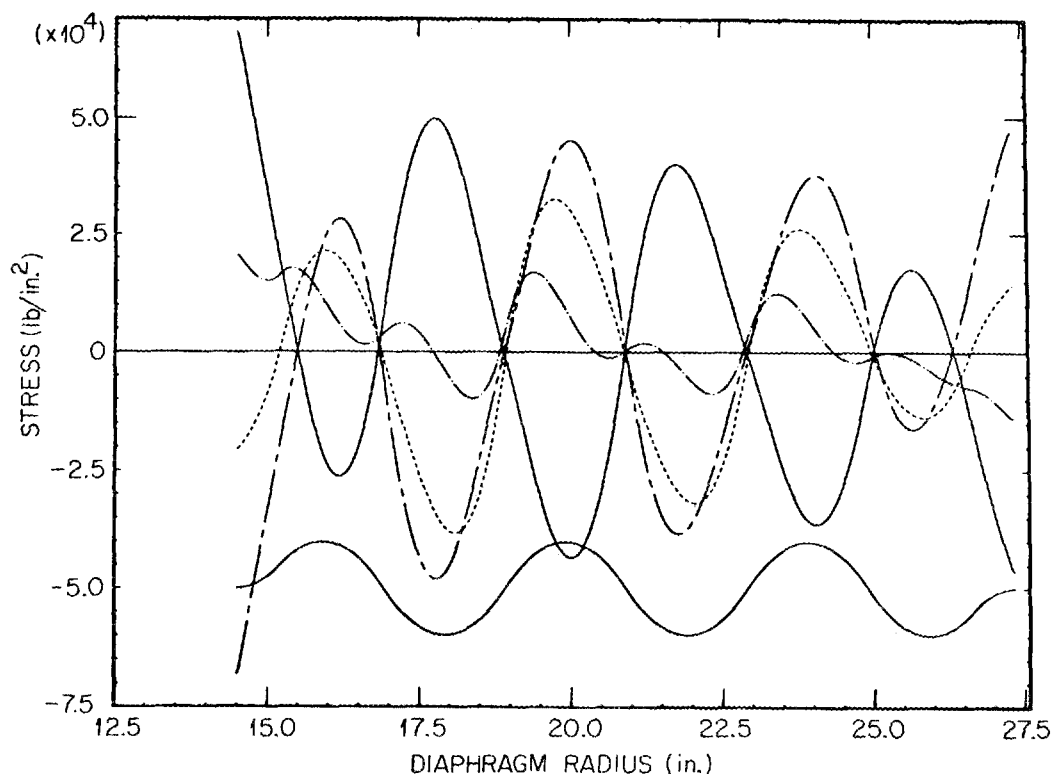


Fig. 6. Case 11, best amplitude.

60 000 psi) over the existing diaphragm case. Circumferential stresses show a similar decrease. These stress values are considered still too high for an effective design.

Cases 3 and 7 had twelve extrema and the same OR as the previous cases. Force requirements for the 1.5-in. displacement were 350 and 450 lb respectively. Case 3, with a 0.151-in. amplitude, showed maximum effective stresses of 59 000 psi, while case 7, with a 0.1-in. amplitude, showed maximum effective stresses of 91 000 psi. Increasing the number of extrema did not give a diaphragm with better characteristics.

Case 9 had only three extrema. The ratio of wavelength to amplitude was the same as case 7. The calculation failed at 1.2-in. deflection under a load of around 400 lb. This failure is an artifact of the method NEPSAP uses to load the diaphragm. Many of the diaphragms studied exhibited an intermediate state where the force went through a local maximum such that larger displacements required somewhat smaller forces until the force increased again when the available metal was stretched nearly flat. Hence, displacement vs force was not monotonic. Since NEPSAP could only add increments of force, these states represented an instability that caused the calculation to fail. This instability was erroneously called a "buckling" condition. It should be understood, however, that it does not represent a failure of the diaphragm, but only a failure of the calculation. The noted sharp increase in force requirement generally follows the calculated displacement corresponding to a theoretically flattened diaphragm, shown as a function of corrugation amplitude in Fig. 7. The 12 series had ten extrema and the 50 series had six extrema.

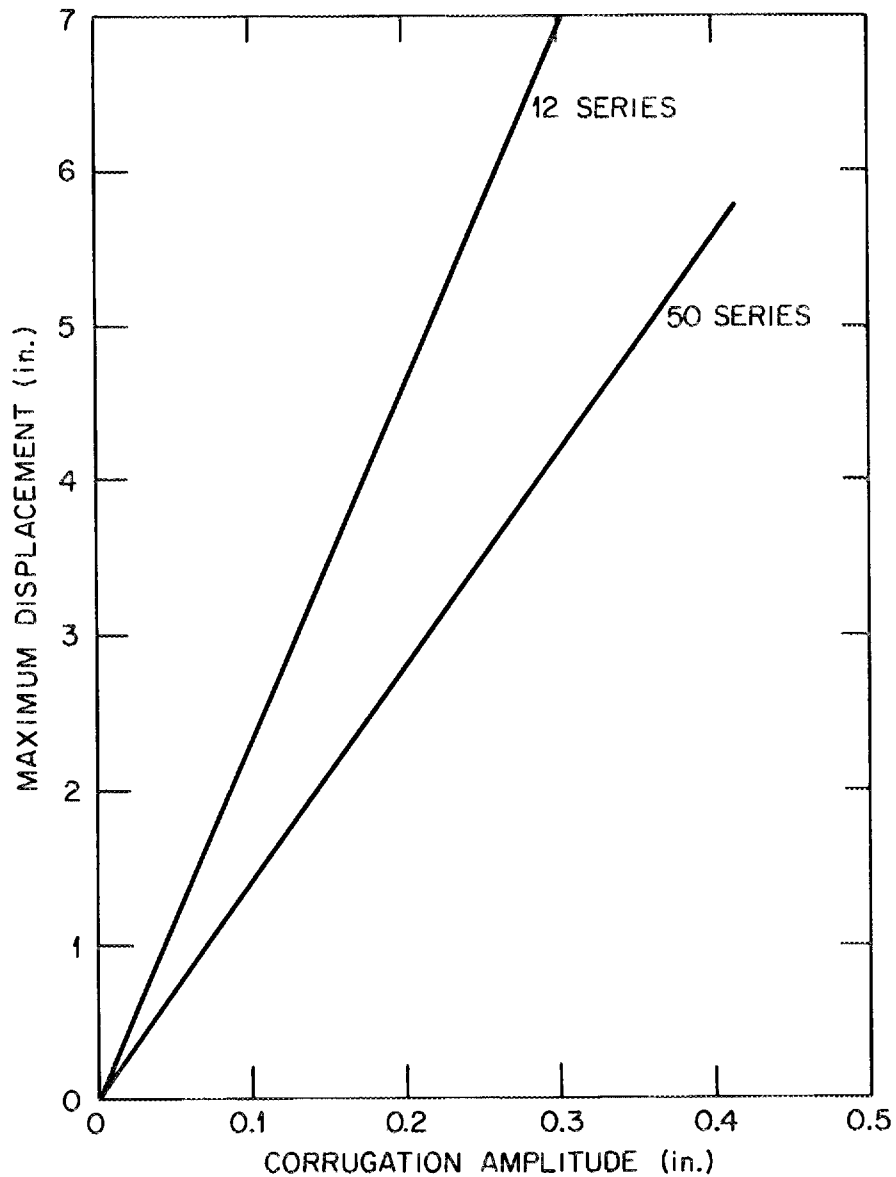


Fig. 7. Maximum displacement.

### 3.3 Larger Radius Diaphragms

In order to reduce the stresses to an acceptable level, it appeared necessary to increase the outside radius. Because the seal must be replaced remotely, it is desirable to keep the diaphragm radius from becoming excessive. A radius of 70.7 in. was used. Three cases (12, 16, and 17) were chosen with a half wavelength of 2 in. and ten extrema [Fig. 2(c)]. Force vs displacement was calculated, and the results are shown in Fig. 8. All three cases required <300 lb of force for a 1.5-in. extension. Case 12 had an amplitude of 0.2 in. and its stress plot is shown in Fig. 9 (full-scale prototype). The maximum stresses at 1.5-in. extension

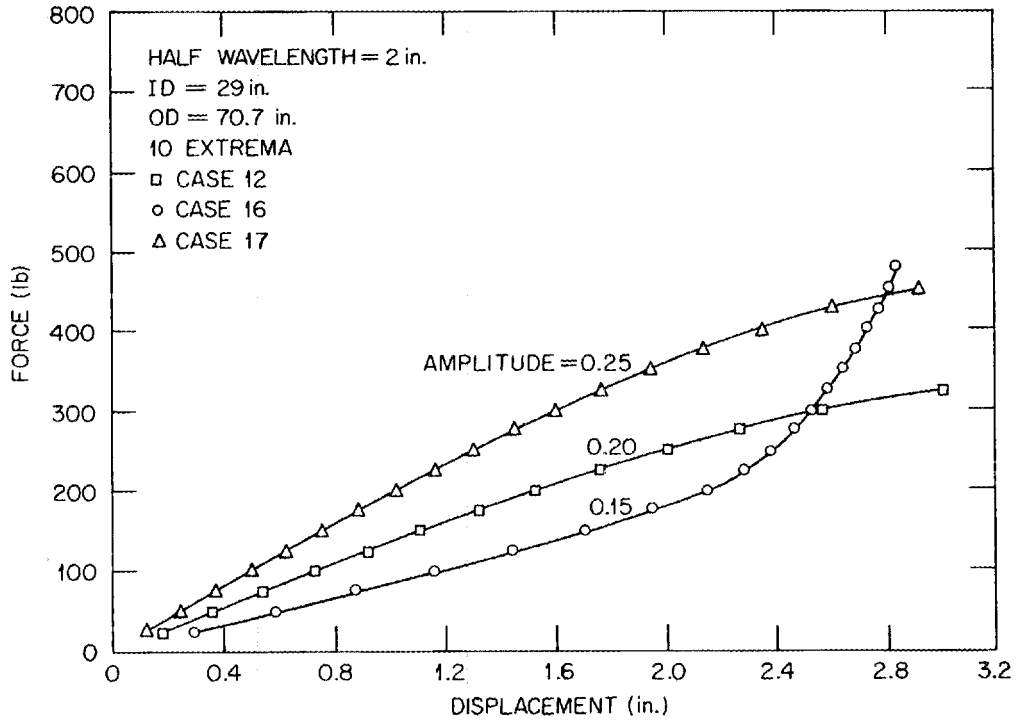


Fig. 8. Force requirement.

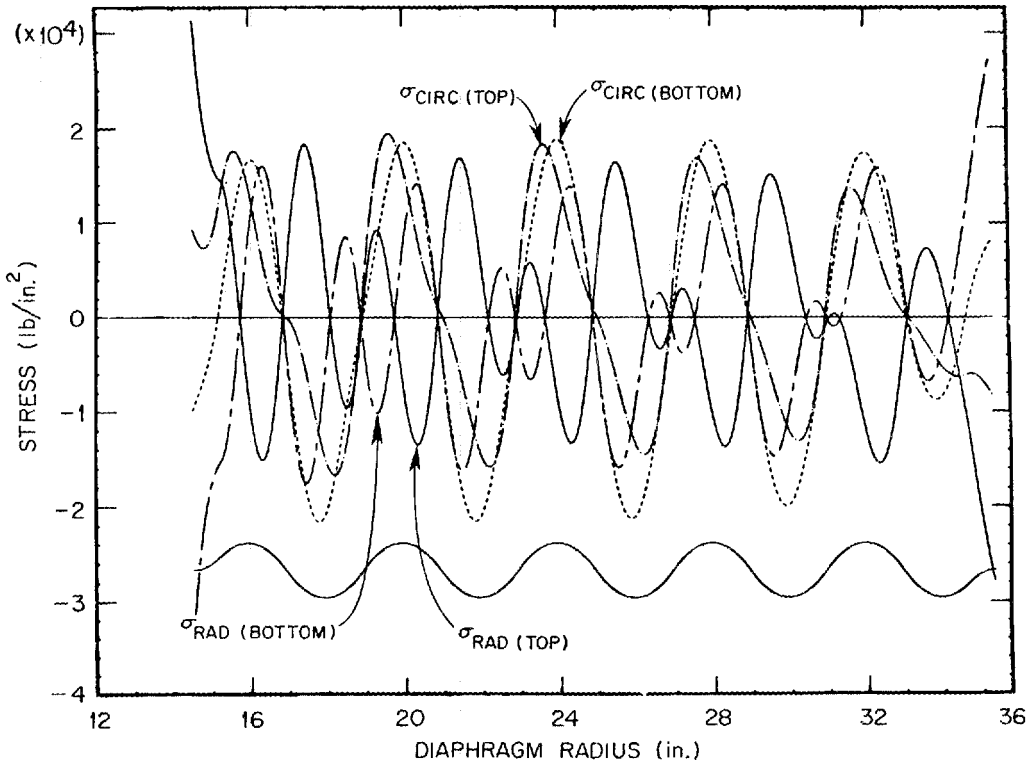


Fig. 9. Case 12, full-scale prototype.

have been reduced to 20 000 psi except at the ends. By chamfering the IR and OR diaphragm clamp rings, these end effects should be minimized.

An interesting presentation of the stress data is seen by constructing Lissajous type curves as seen in Fig. 10. Here the top and bottom surface stresses at 1.5-in. displacement are plotted as a function of the corrugation amplitude. The maximum tensile and compressive

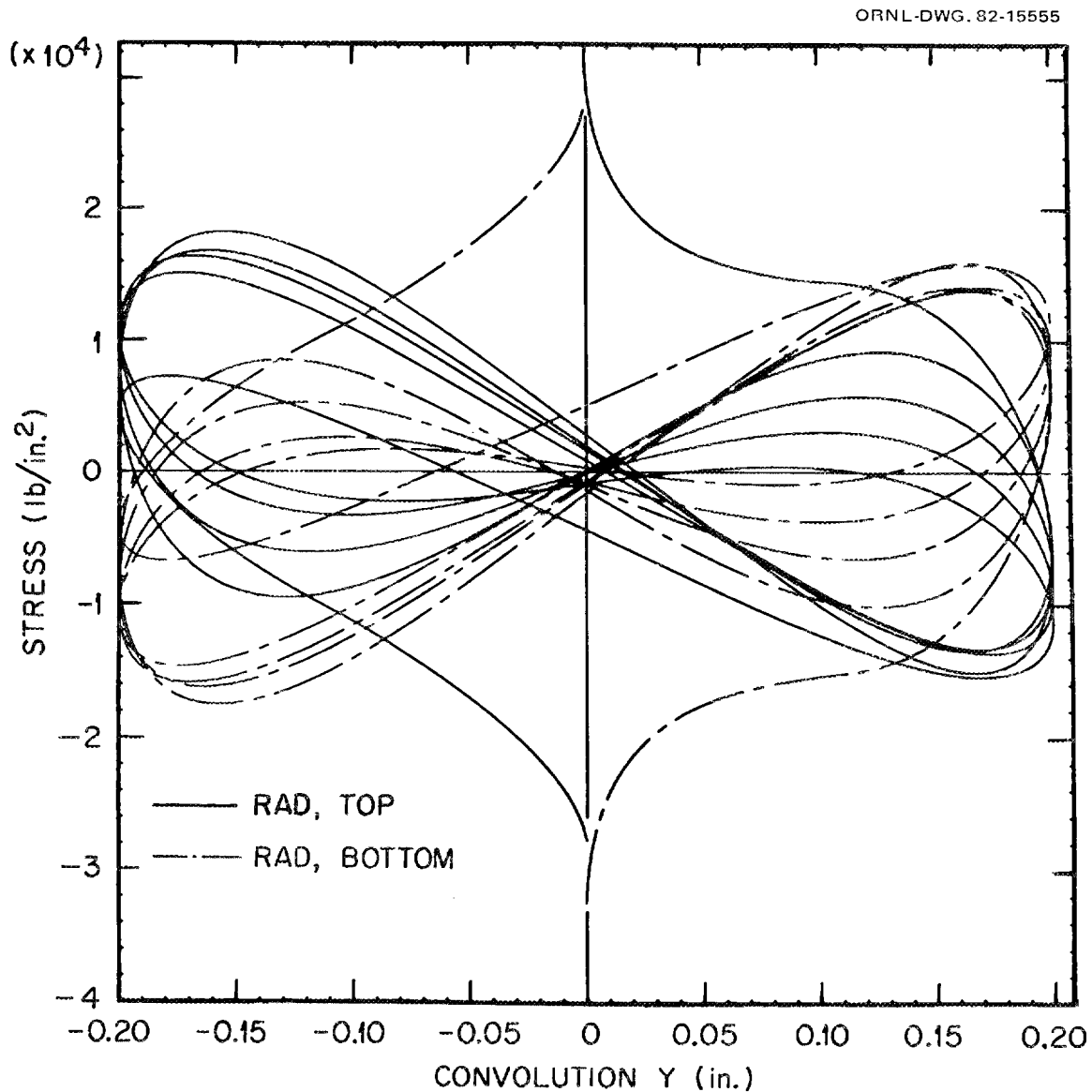


Fig. 10. Lissajous curves of radial stresses, case 12, full-scale prototype.

stresses are seen to occur near the extrema. Figure 11 shows the Lissajous curves of circumferential surface stresses. Here the maximum stress is near each extremum with alternate extrema in tension.

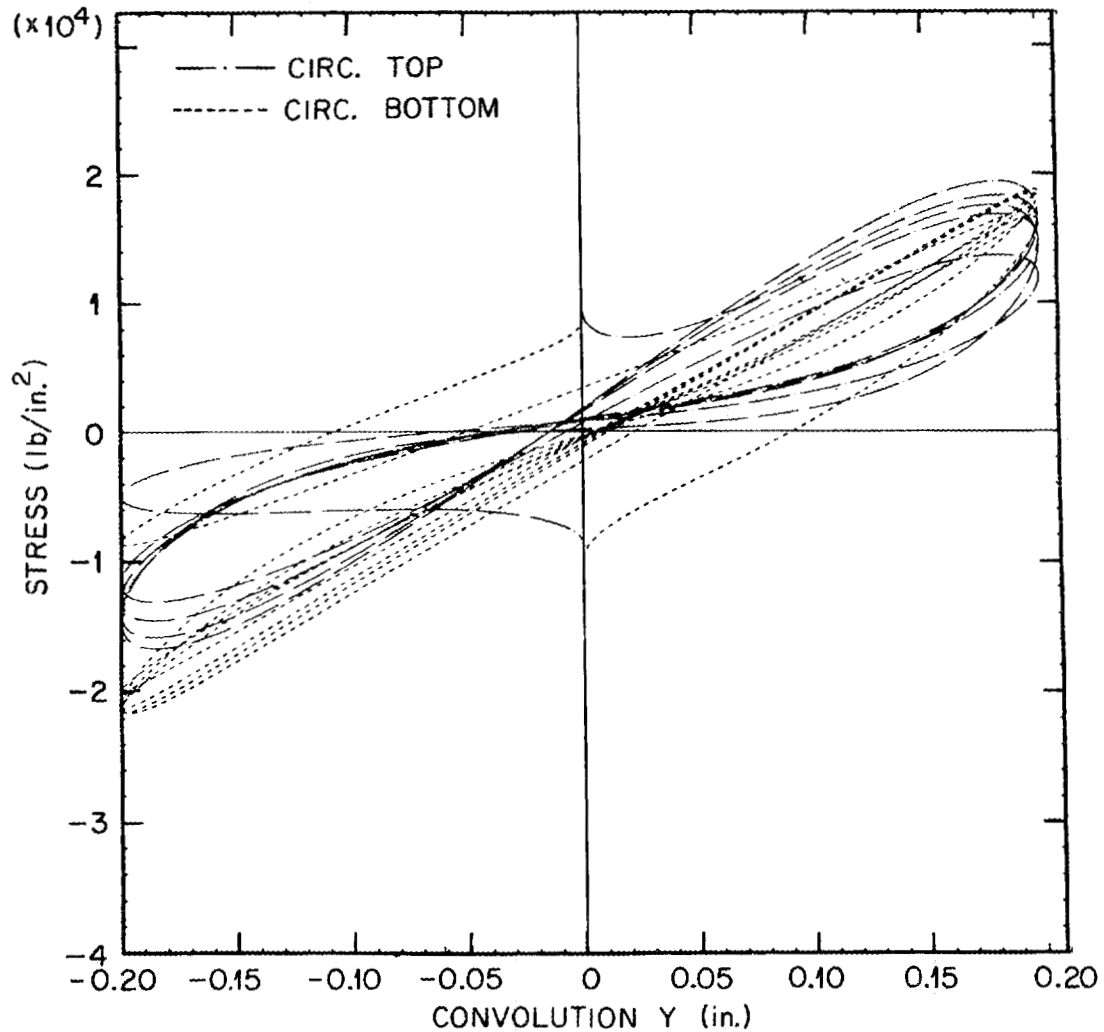


Fig. 11. Lissajous curves of circumferential stresses, case 12, full-scale prototype.

### 3.4 Alternate Design

Our investigations have shown there are very few fabricators of diaphragms of this size. Although case 12 resulted in a satisfactory diaphragm, we studied an alternate diaphragm with six instead of ten extrema which might be easier to fabricate. Using the same IR and OR as case 12, we lengthened the half wavelength to 3.25 in. and calculated force requirements as a function of amplitude and displacement. Figure 12 shows the results of calculations for cases 50 through 54 and 56. The force required for 1.5-in. displacement, case 53, was 150 lb compared to 200 lb for a ten extrema diaphragm with the same amplitude. For all cases with amplitudes between 0.13 and 0.25 in. the calculations failed by buckling before the 1.5-in. displacement was reached. An interesting result is shown for a flat diaphragm. Almost no force was required to displace the diaphragm the first 0.75 in., but over the next 0.5 in. this force increased very rapidly to 600 lb.

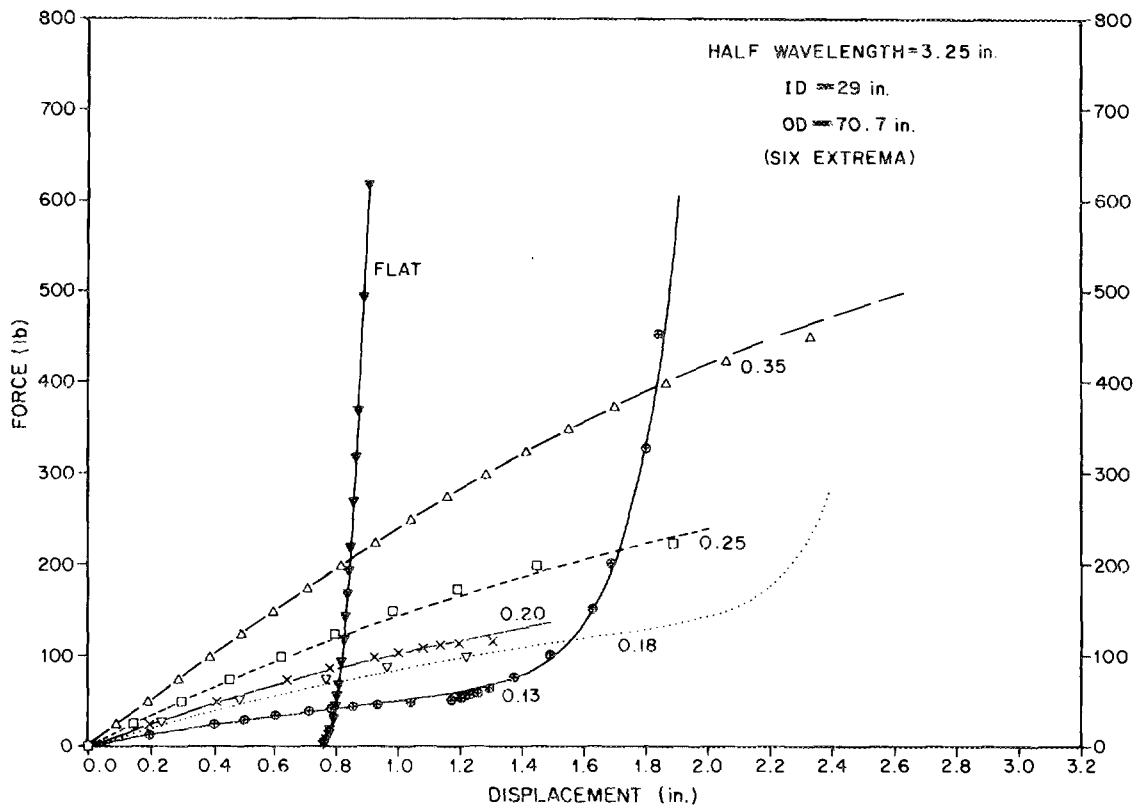


Fig. 12. Force requirement.

Stress plots at 1.5-in. displacement of cases 51 and 56 are shown in Fig. 13(a) and (b) for comparison. Case 51, with an amplitude of 0.25 in., was in a nearly linear region of the force vs displacement curve and had many maxima of stresses across the diaphragm. Case 56, with an amplitude of 0.13 in., was in a region where the force was sharply increasing. The number of stress maxima was less than case 51 with the top surface radial stress maxima coinciding with the extrema.

### 3.5 Scaled Design

To test the larger diameter diaphragms in a test stand, it would be convenient to scale down the dimensions. Calculations were made to design a 3/4 (0.75)-scale version of case 12. The results, shown in Table 3, compare dimension and stress values for the scaled version, case 14, with case 12. Dimensions, including thickness and amplitude, are 0.75 times the values for case 12. To arrive at the same stress values for the scaled version, it is displaced 0.75 of the distance of the larger diaphragm. The force required is proportional to the square of the scaling factor  $(0.75)^2$ . The stress value shown is the calculated maximum radial surface stress in compression.

### 3.6 Reverse Displacement

The standard stress and force calculations were made with inside radii moving in the upward direction in Fig. 2. Force was applied in the opposite direction and displacement

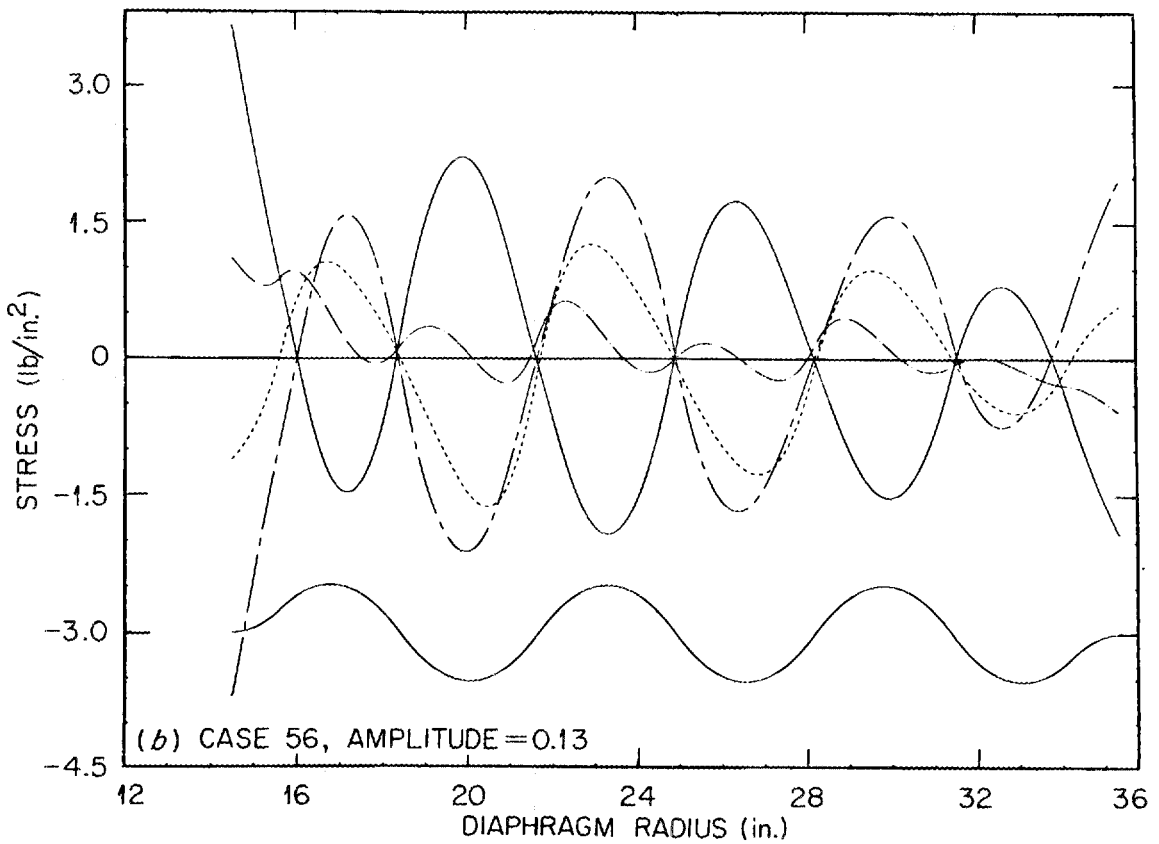
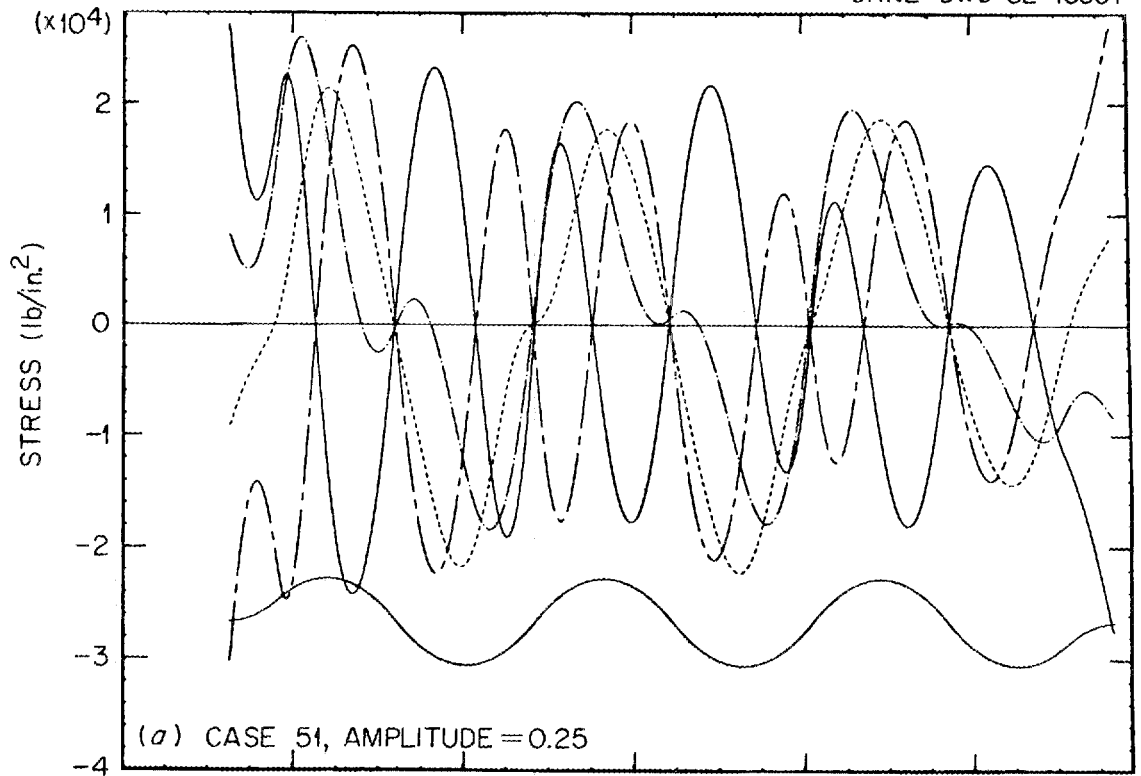


Fig. 13. Stress plots for cases 51 and 56.

Table 3. Scaled design

Case number	12	14
Scale factor	1	0.75
Inside radius, in.	14.5	10.88
Outside radius, in.	35.338	26.50
Amplitude, in.	0.2	0.15
Thickness, in.	0.018	0.014
Extrema	10	10
Deflection, in.	1.5	1.125
Force, lb	196	110.3
Stress, psi	$-33.2 \times 10^3$	$-33.2 \times 10^3$

values obtained for cases 12 and 13. The results are plotted in Fig. 14. Case 12 has full corrugations and gave a nearly symmetric curve. With a force requirement of under 400 lb for a displacement of 3 in., case 13 had flats at the IR and the OR. The force requirement was much greater, and the diaphragm was markedly stiffer when displaced in the negative direction.

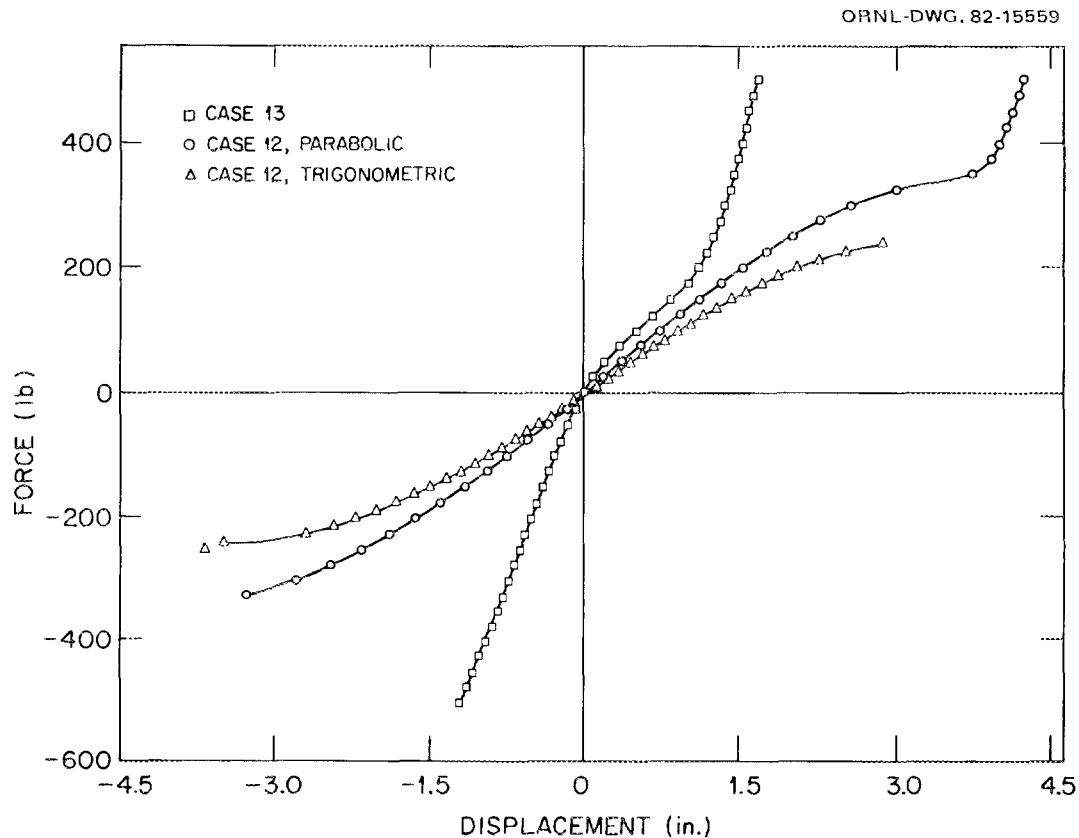


Fig. 14. Force vs displacement.

## 3.7 Measured Stresses

Stresses were measured on the existing diaphragm at four radial locations to compare with the calculated values. A pair of strain gages placed at right angles to each other at each position allowed measurement of both the radial and circumferential strains. The radial positions are shown on the diaphragm profile in Fig. 15. Four pairs of strain gages were

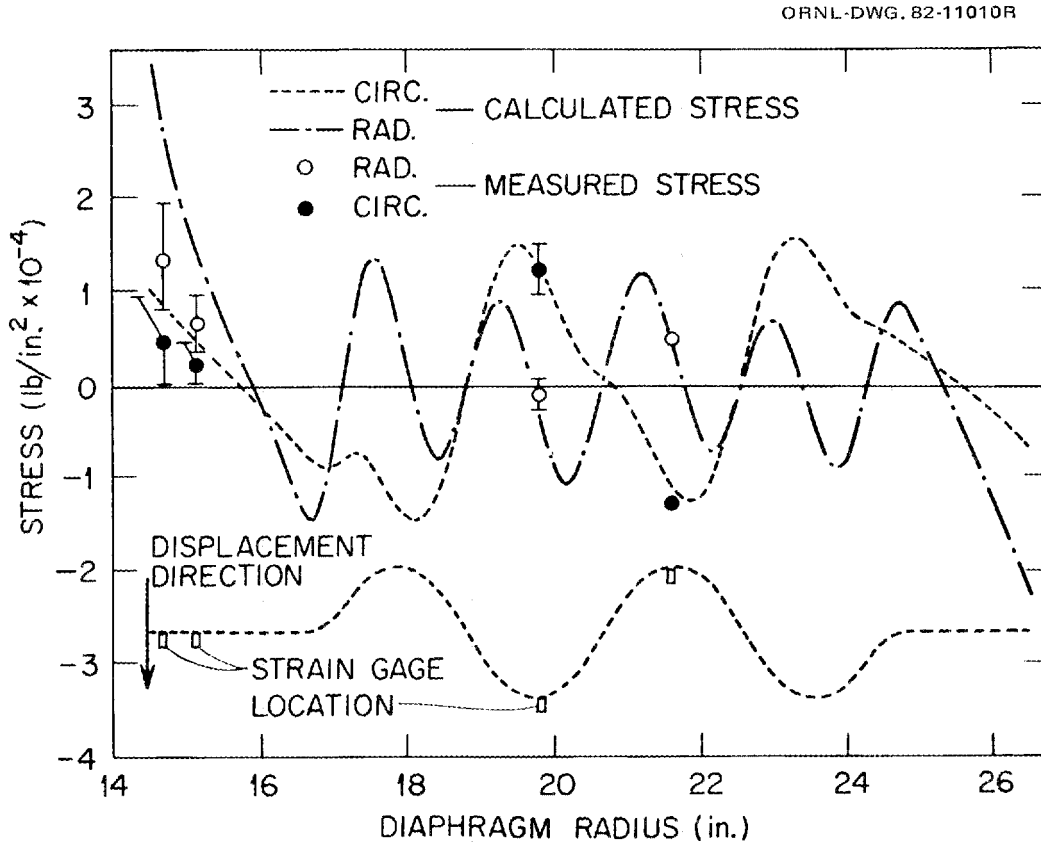


Fig. 15. Measured and calculated stresses.

attached at each radial position on the inner flat portion of the diaphragm. Each pair was spaced  $90^\circ$  apart. Two pairs of strain gages were attached  $180^\circ$  apart at a radius of 19.76 in., and a final pair on an extrema at a radius of 21.63 in. Readings were taken of strain as the inner diaphragm ring was displaced 0.5 in. The inner bearing flange was rotated  $180^\circ$  and the test repeated to average out any affect of nonalignment. The radial stresses were calculated from the strain values by the expression:

$$\sigma_R = \frac{E}{(1 - \alpha^2)} (\epsilon_R + \alpha\epsilon_C) \times 10^{-6} ,$$

where

$\sigma_R$  = radial stress, psi;

$E$  = Young's modulus ( $29 \times 10^6$  psi);

$\alpha$  = Poisson's ratio (0.3);

$\epsilon_R$  = radial strain,  $\mu\text{in./in.}$ ;

$\epsilon_C$  = circumferential strain,  $\mu\text{in./in.}$

The circumferential stresses were similarly calculated. These results are given in Table 4. The average measured values are shown on a plot of the calculated stresses in Fig. 15. Good agreement between measured and calculated stresses are seen at the extrema locations. The

**Table 4. Comparison of calculated and measured stresses**

Radius (in.)	Radial stress ( $10^4$ psi)			Circumferential stress ( $10^4$ psi)		
	Calculated	Measured	$\sigma^a$	Calculated	Measured	$\sigma^a$
14.68	2.779	1.346	0.624	0.868	0.471	0.417
15.18	1.291	0.623	0.369	0.418	0.216	0.218
19.76	-0.28	-0.072	0.123	1.302	1.183	0.239
21.63	0.306	0.44		-1.184	-1.23	

<sup>a</sup> $\sigma$  = standard deviation, measured results.

measured values are lower than the calculated values on the flat region of the diaphragm near the inner radius. The model used for the calculations assumes no deformation of the inner clamp ring and a sharp  $90^\circ$  corner on the ring. One would expect these assumptions to give a higher calculated stress.

#### 4. CONCLUSIONS

The work reported here supports the following conclusions:

1. The requirements for a diaphragm for a rotary seal at the discharge end of the CFRP prototypic voloxidizer are satisfied by case 12 of this study. Specifically, the force required to displace the inner radius 1.5 in. in either direction is less than 400 lb, and the stresses developed in the diaphragm are low enough to allow it to be flexed through hundreds of cycles without failure.
2. If a displacement of 1.5 in. is a requirement for a Provol application, a diaphragm  $>54.6$ -in. diam is required to obtain the necessary characteristics of stiffness and acceptable stresses.

3. This study has addressed a general problem of diaphragm design, examining thickness, outer radius, corrugation wavelength and corrugation amplitude as variables, and has established the general effect of each on stiffness and stresses, comprising a basis for the selection of diaphragms for similar applications.
4. For a given diaphragm, varying only the amplitude of the corrugations, it was found that the initial stiffness decreases with decreasing amplitude. However, at very small amplitudes the maximum displacement is limited as the metal stretches flat.
5. The NEPSAP computer program has proved to be a very good tool for the evaluation of diaphragm designs. The program plus peripheral computer programs developed to generate input and process output comprise an available methodology for diaphragm development in the event that additional effort becomes desirable in the future.
6. Limited experimental measurements validate the stress values calculated by NEPSAP for meaningful locations on a diaphragm surface.

## 5. ACKNOWLEDGMENTS

The authors wish to thank S. K. Iskander, Computer Sciences Division, and J. Mayhall, UCC-ND Engineering, for their help in the computer modeling. Also, our thanks to D. Aldrup, co-op student from the University of Alabama for the force plot programming and D. J. Kington for the strain measurements. We would further like to acknowledge the invaluable contributions of M. J. Rennich who was the principal engineer on our project, is co-holder of the patent on the voloxidizer seal, and who pursued the design and procurement of the experimental diaphragm and test facilities used in this work.

## REFERENCES

1. K. J. Bathe, *ADINA – A Finite Element Program for Automatic Dynamic Incremental Non-Linear Analysis*, Rpt 82448-1, Massachusetts Institute of Technology (May 1977).
2. S. K. Iskander (Oak Ridge National Laboratory), personal communication to M. E. Whatley, September 1980.
3. Parviz Sharifi, *User's Manual for NEPSAP*, Huntsville Research and Engineering Center (August 1974).
4. J. G. Morgan, *Operational Testing of a Rotary Seal for a Proposed Voloxidizer for a Fuel Recycle Plant*, ORNL/TM-8289 (April 1982).
5. *Mechanical and Physical Properties of Austenitic Chromium-Nickel Stainless Steels at Ambient Temperatures*, The International Nickel Company, Inc., 1963.



APPENDIX A

PROGRAM FOR MATRIX GENERATION

```
C ** THIS GENERATES A MATRIX OF POINTS ON THE SURFACES OF A DIAPHRAM
C ** FOR INPUT TO NEPSAP
C ** FOR USE IN STRESS CALCATIONS
C ** VERSION MARCH 8, 1982
C
```

```
    DIMENSION CASE(3),XX(5000),YYY(5000)
    DO 55 KASE=1,100
    READ(11,200,END=30) NCON,R,P,ZZZ,ZLG,AF,THK,STP,CASE
200  FORMAT(I4,7E8.2,3A4)
    WRITE(12,121) CASE
121  FORMAT(3X,3A4,' ****')
    WRITE(12,120) NCON,R,P,ZZZ,ZLG,AF,THK,STP
120  FORMAT(' DIAPHRAM IS DEFINED BY: '/I5,' CONVOLUTIONS' /
1 ' RADIUS OF INNER SUPPORT =',F8.3/
2 ' RADIUS TO FIRST EXTREMA =',F8.3/
3 ' RADIUS TO OUTER SUPPORT =',F8.3/
4 ' HALF WAVE LENGTH =',F8.3,' AND AMPLITUDE =',F6.3/
5 ' DIAPHRAM THICKNESS =',F7.4,5X,' MESH INCREMENT IS',F5.2,
6 ' TIMES THICKNESS')
    TO2=THK/2.
    XSTP=THK*STP
    SQ2=.5*SQRT(2.)*ZLG
    XO=P-SQ2
    XI=P-.5*SQ2
    XG=P+(NCON-1)*ZLG + .5*SQ2
    XF=P+(NCON-1)*ZLG + SQ2
    WRITE(12,130) XO,XF
130  FORMAT(' RADIUS TO FIRST CURVATURE =',F8.3/
1 ' RADIUS TO LAST CURVATURE =',F8.3)
    IF(XO.LT.R .OR. XF.GT.ZZZ) GOTO 31
    CF=4.*AF/ZLG/ZLG
    X=R
```

```
C
    DO 20 NPT=1,5000,2
    IF(X.GT.XO) GOTO 1
C  FLAT REGION BEFORE FIRST CURVING
    Y=0.
    DYX=0.
    GOTO 10
    1 IF(X.GT.XI) GOTO 2
C  INITIAL CURVING
    Y=CF*(X-XO)*(X-XO)
    DYX=2.*CF*(X-XO)
    GOTO 10
    2 IF(X.GT.XG) GOTO 3
C  WE ARE NOW ON CURVE ASSOCIATED WITH EXTREMA N
    N= 1.5+(X-P)/ZLG
    SGN= (-1.)**(N-1)
    TT= X-P-(N-1)*ZLG
C  Y IS THE CENTER OF THE DIAPHRAM AT X
    Y= AF-CF*TT*TT
    Y=SGN*Y
C  DYX IS THE FIRST DERIVATIVE OF THE CURVE
    DYX=-2.*SGN*CF*TT
    GOTO 10
    3 IF(X.GT.XF) GOTO 4
```

```

C WE ARE ON FINAL CURVE
  Y=SGN*CF*(X-XF)*(X-XF)
  DYX=SGN*2.*CF*(X-XF)
  GOTO 10
  4 IF(X.GT.ZZZ) GOTO 22
C THIS IS FINAL FLAT
  Y=0.
  DYX=0.
C USE SLOPE TO GET POSITION OF POINTS ON DIAPHRAM
C SURFACE NORMAL TO CURVE AT X,Y.
  10 FCOS=SQRT(1./(1.+DYX*DYX))
  PSIN=DYX*FCOS
  X1=X+TO2*PSIN
  X2=X-TO2*PSIN
  Y1=Y-TO2*FCOS
  Y2=Y+TO2*FCOS
  XXX(NPT)=X1
  YYY(NPT)=Y1
  XXX(NPT+1)=X2
  YYY(NPT+1)=Y2
C CALCULATE APPROXIMATE LENGTH ALONG CURVE FOR NEXT X
C THIS APPROXIMATION EMBODIES A SECOND ORDER ERROR
C THAT DECREASES WITH INCREMENT SIZE AND AMPLITUDE.
  DXS=THR*STP*FCOS
  X=X+DXS
  20 CONTINUE
  22 NPT=NPT-1
  WRITE(12,122) NPT
  122 FORMAT(' THERE WERE ',I4,' NODES GENERATED'/)
  DO 23 M=1,NPT
C THIS OUTPUT IS IN CORRECT FORMAT FOR INPUT TO WEPSAP
  WRITE(12,111) M,XXX(M),YYY(M)
  23 CONTINUE
  111 FORMAT(15,30X,2F10.5)
  55 CONTINUE
  30 STOP
  31 TYPE 310
  310 FORMAT (' YOU HAVE AN IMPOSSIBLE CASE')
  STOP
  END

```

## APPENDIX B

## MATRIX PROGRAM OUTPUT

KASE 54 \*\*\*\*\*  
 DIAPHRAM IS DEFINED BY:  
 6 CONVOLUTIONS  
 RADIUS OF INNER SUPPORT = 14.500  
 RADIUS TO FIRST EXTREMA = 16.800  
 RADIUS TO OUTER SUPPORT = 35.338  
 HALF WAVE LENGTH = 3.248 AND AMPLITUDE = 0.180  
 DIAPHRAM THICKNESS = 0.0180 MESH INCREMENT IS 2.00 TIMES THICKNESS  
 RADIUS TO FIRST CURVATURE = 14.503  
 RADIUS TO LAST CURVATURE = 35.337  
 THERE WERE 1168 NODES GENERATED

1	14.50000	-0.00900
2	14.50000	0.00900
3	14.53604	-0.00893
4	14.53596	0.00907
5	14.57208	-0.00868
6	14.57192	0.00932
7	14.60813	-0.00825
8	14.60787	0.00975
9	14.64417	-0.00765
10	14.64382	0.01035
11	14.68020	-0.00687
12	14.67977	0.01113
13	14.71624	-0.00591
14	14.71572	0.01208
15	14.75227	-0.00478
16	14.75166	0.01321
17	14.78829	-0.00346
18	14.78759	0.01452
19	14.82431	-0.00198
20	14.82352	0.01601
21	14.86032	-0.00031
22	14.85944	0.01767
23	14.89632	0.00153
24	14.89536	0.01950
25	14.93231	0.00354
26	14.93126	0.02151
27	14.96829	0.00574
28	14.96715	0.02370
29	15.00427	0.00811
30	15.00304	0.02606
31	15.04023	0.01065
32	15.03891	0.02860
33	15.07617	0.01337
34	15.07477	0.03132
35	15.11211	0.01626
36	15.11062	0.03420
37	15.14803	0.01933
38	15.14645	0.03726
39	15.18393	0.02258
40	15.18227	0.04050
41	15.21982	0.02600
42	15.21807	0.04391
43	15.25570	0.02959
44	15.25386	0.04749
45	15.29155	0.03335
46	15.28963	0.05125
47	15.32739	0.03729
48	15.32538	0.05518
49	15.36321	0.04140
50	15.36111	0.05928
51	15.39900	0.04569



*INTERNAL DISTRIBUTION*

- |                      |                                 |
|----------------------|---------------------------------|
| 1. S. M. Babcock     | 22. R. E. Norman                |
| 2. E. C. Bradley     | 23. F. L. Peishel               |
| 3--5. W. D. Burch    | 24. R. L. Philippone            |
| 6. R. V. Clark       | 25. T. W. Semple                |
| 7. D. J. Crouse      | 26. J. H. Shaffer               |
| 8. J. H. Evans       | 27. B. B. Spencer               |
| 9. M. J. Feldman     | 28. J. G. Stradley              |
| 10. W. S. Groenier   | 29. O. K. Tallent               |
| 11. T. L. Hebble     | 30. V. C. A. Vaughen            |
| 12. J. N. Herndon    | 31. T. D. Welch                 |
| 13. E. H. Kreig, Jr. | 32--41. M. E. Whatley           |
| 14. R. E. Leuze      | 42. O. O. Yarbrow               |
| 15. B. E. Lewis      | 43--44. Laboratory Records      |
| 16. A. L. Lotts      | 45. Laboratory Records, ORNL-RC |
| 17--21. J. G. Morgan | 46. ORNL Patent Office          |

*EXTERNAL DISTRIBUTION*

- 47--48. K. O. Laughon, Jr. Acting Director, Office of Spent Fuel Management and Reprocessing Systems, U.S. Department of Energy, Washington, DC 20545
49. F. P. Baranowski, 1110 Dapple Grey Court, Great Falls, VA 22066
50. S. J. Beard, Vice President, Engineering and Technology, Exxon Nuclear Company, Inc., 2101 Horn Rapids Road, Richland, WA 99352
51. M. J. Ohanian, Associate Dean for Research, College of Engineering, 300 Weil Hall, University of Florida, Gainesville, FL 32611
52. J. F. Proctor, Senior Technical Specialist, Petrochemicals Department, Atomic Energy Division, E. I. du Pont de Nemours and Company, Montchanin Building 6600, Wilmington, DE 19898
53. Office of Assistant Manager for Energy Research and Development, DOE-ORO, Oak Ridge, TN 37830
- 54--144. Given distribution as shown in TIC-4500 under UC-86, Consolidated Fuel Reprocessing Category